Direct Access to Mesoporous Crystalline TiO_2/Carbon Composites with Large and Uniform Pores for Use as Anode Materials in Lithium Ion Batteries[a]

Jinwoo Lee, Yoon S. Jung, Scott C. Warren, Marleen Kamperman, Seung M. Oh, Francis J. DiSalvo, Ulrich Wiesner*

Mesoporous and highly crystalline TiO_2 (anatase)/carbon composites with large (>5 nm) and uniform pores were synthesized using PI-*b*-PEO block copolymers as structure directing agents. Pore sizes could be tuned by utilizing block copolymers with different molecular weights. The resulting mesoporous TiO_2/carbon was successfully used as an anode material for Li ion batteries. Without addition of conducting aid (Super P), the electrode showed high capacity during the first insertion/desertion cycle due to carbon wiring inside the walls of mesoporous TiO_2/carbon. The electrode further showed stable cycle performance up to 50 cycles and the specific charge capacity at 30 C was 38 mA h (g of TiO_2)$^{-1}$, which indicates CCM-TiO_2/carbon can be used as a material for high rate use.

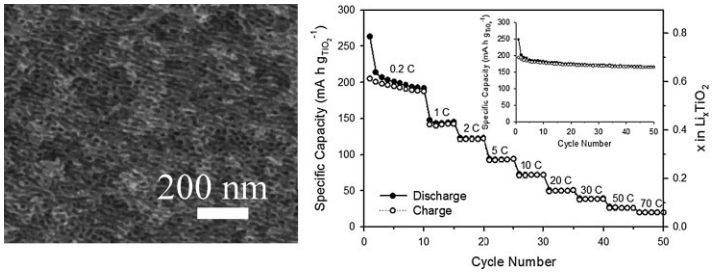

Introduction

Transition metal oxides are expected to enhance performance levels of various energy storage devices, such as lithium ion batteries and fuel cells.[1] For example, to improve the catalytic performance in fuel cells, the electrodes were recently modified with transition metal oxides, such as TiO_2, CeO_2, and WO_3.[2] Several transition metal oxides, including TiO_2, SnO_2, and V_2O_5 have been considered as promising electrode materials for lithium secondary batteries.[3] For example, nanostructured TiO_2 materials have been employed as anode materials for lithium ion insertion.[4] The high reaction potential (ca. 1.6–2.1 V vs. Li/Li$^+$) of TiO_2 over the already-commercialized graphite provides two important advantages:[5] (i) Li plating on the surface of anode materials can be avoided, constituting an important safety consideration. (ii) Because of negligible side reactions above 1.0 V (vs. Li/Li$^+$), high surface area TiO_2 can be employed as the anode for high rate applications.

Conceptually, mesoporous transition metal oxide/carbon composites are expected to be very useful as electrode

U. Wiesner, S. C. Warren, M. Kamperman
Department of Materials Science and Engineering, Cornell University, Ithaca, New York 14853, USA
E-mail: ubw1@cornell.edu
J. Lee
Department of Chemical Engineering/School of Environmental Science and Engineering, Pohang University of Science and Technology, Kyungbuk 790-784, Korea
Y. S. Jung, S. M. Oh
Department of Chemical and Biological Engineering, and Research Center for Energy Conversion & Storage, Seoul National University, Seoul 151-744, Korea
F. J. DiSalvo
Department of Chemistry, Cornell University, Ithaca, NY 14853, USA

[a] Supporting information for this article is available at the bottom of the article's abstract page, which can be accessed from the journal's homepage at http://www.mcp-journal.de, or from the author.

DOI: 10.1002/macp.201000687

materials, due to the electrical conductivity of carbon and electrochemical functionality of transition metal oxides. Recently, silicon-based anode materials have been described, but these approaches require cumbersome cost-ineffective deposition techniques and are usually plagued with low cycling capacity.[6] In order to improve relevance for applications, the synthesis approach should be simple and cost-effective. Usually, transition metal oxide/carbon composites have been fabricated by post-deposition of transition metal oxide nanoparticles on already synthesized nanostructured carbon materials.[7] However, this requires very tedious multi-steps in order to make the nanostructured composite and to incorporate the transition metal oxides. Specifically, the process to make metal oxide nanoparticles dispersed on ordered mesoporous carbons[7b–d] is composed of more than nine steps over 10 d to get the final composite materials.

Several research groups have synthesized pure mesoporous titanium dioxide using commercially available P123 ($(EO)_{20}(PO)_{70}(EO)_{20}$).[8] Very recently, Zhao and co-workers reported on the synthesis of mesoporous TiO_2/carbon composites using commercially available Pluronic P123 block copolymers without further electrochemical characterization. While suggesting an interesting approach, the pore size of the resulting materials was smaller than 3.5 nm.[9] In order to provide easy access of electrolyte molecules to such a functional composite in diverse applications, it is desirable, however, to generate mesoporous transition metal oxides/carbon composite with large (>5 nm) and uniform pores.[10]

Herein, we report on the direct synthesis of mesoporous and highly crystalline TiO_2 (anatase)/carbon composites with large (>5 nm), tunable and uniform pores and their performances as anodes in Li ion batteries. Well-defined conducting carbon/transition metal oxide composites were synthesized through a simple synthetic route for use as electrode materials. Synthesis was achieved by the assembly of poly(isoprene-*block*-ethylene oxide) (PI-*b*-PEO) block copolymers with varying molecular weights with titanium dioxide sols and carbon precursors, furfuryl alcohol (FA) or resol nanoparticles,[11] which selectively swell the hydrophilic PEO block of the block copolymers. A non-hydrolytic sol–gel route to metal oxides was employed to make TiO_2 sols.[12] PI-*b*-PEO block copolymers were synthesized in our laboratory with controllable molecular weights. PI-*b*-PEO was used since it is well established as a model system for the study of mesoporous materials synthesis.[13]

Experimental Part

Synthesis of Cornell Composition of Matters (CCM)-TiO_2/Carbon-1

PI-*b*-PEO-1 was used with $\overline{M}_n = 27\,220\ g \cdot mol^{-1}$ and 16.7 wt.-% PEO. After 0.2 g of PI-*b*-PEO was dissolved in 2 mL tetrahydrofuran (THF), 0.53 mL of titanium tetraisopropoxide (TTIP), and 0.21 mL titanium chloride (IV) were added into the solution. After stirring for 1 h at room temperature, 0.5 g of FA was added and stirred for more than 12 h at room temperature. Films were cast by evaporation of the solvent and byproducts in air on a hot plate at 50 °C and then at 130 °C in a vacuum oven for one hour. During heat-treatment at 50 °C under air and subsequently at 130 °C under vacuum, the FA is polymerized in hydrophilic block copolymer domain. The as-synthesized amorphous material was heat treated to 700 °C using $1\ °C \cdot min^{-1}$ ramp under argon and held for 2 h or more resulting in crystallization of the amorphous metal oxide walls and conversion of the carbon source to conducting carbon.

While we did not perform the entire method in a single pot (the precursors were mixed in a vial, films were cast on a aluminum dish by evaporation, and finally the films were heat-treated at 700 °C to get final mesoporous TiO_2/carbon material), one can in theory use a single alumina dish (one pot) for each of the processing steps, i.e., mix the precursors, evaporate off the solvents to obtain a thin film, and still use the same dish for the subsequent heat treatments.

Synthesis of CCM-TiO_2/Carbon-2

PI-*b*-PEO was used with $\overline{M}_n = 15\,640\ g \cdot mol^{-1}$ and 13.9 wt.-% PEO. After 0.2 g of PI-*b*-PEO was dissolved in 2 mL THF, 0.53 mL of TTIP, and 0.21 mL titanium chloride (IV) were added into the solution. After stirring for more than 1 h at room temperature, 0.24 g of resol[11] was added and stirred for more than 12 h at room temperature. The $\overline{M}_n$ of resol was $\approx 300\ g \cdot mol^{-1}$. The remaining process step was the same as described before.

Synthesis of Pure Mesoporous TiO_2, CCM-TiO_2

PI-*b*-PEO-1 was used with $\overline{M}_n = 27\,220\ g \cdot mol^{-1}$ and 16.7 wt.-% PEO. After 0.2 g of PI-*b*-PEO was dissolved in 2 mL THF, 0.71 mL of TTIP, and 0.27 mL titanium chloride (IV) were added into the solution. The remaining process step was the same as described before, except heat treatment was at 450 °C for 2 h under air.

Electrochemical Characterization

A 2032-type coin cell was employed to assess the electrochemical performance of anatase TiO_2 electrodes. The composite electrodes were prepared by spreading a slurry mixture of active material, Super P (MMM Co., as a carbon additive for conductivity enhancement) and polyvinylidene fluoride (PVdF, as a binder) on a piece of copper foil (as a current collector, apparent area = 1 cm^2). The electrodes were then dried at 120 °C under vacuum for 12 h, and subsequently pressed in order to enhance the inter-particle contact and to ensure a better adhesion to the current collector. Lithium foils (Cyprus Co.) were used as the counter and reference electrode, and 1.0 M $LiPF_6$ dissolved in a mixture of ethylene carbonate (EC) and diethyl carbonate (DMC) (1:2 v/v) was used as the electrolyte. The galvanostatic discharge-charge cycling was made at a current density of 0.2 C in the voltage range of 1.0–3.0 V (vs. Li/Li^+) [1 C = 335.5 mA (g of TiO_2)$^{-1}$]. In this paper, the specific current and capacity were expressed on the basis of only the TiO_2 component, and the lithiation was expressed as discharging, whereas the de-lithiation was expressed as charging.

Small angle X-ray scattering (SAXS) experiments were performed on Rigaku RU-H3R copper rotating anode ($\lambda = 1.54$ Å). XRD data was obtained from powdered samples using a Scintag Inc. q–q diffractometer (CuK_α, 1.54 Å). TEM images were recorded on a JEOL 1200 EX at 120 kV. HRTEM images were recorded on an FEI Tecnai G20 TEM at 200 kV. Raman data was collected on a Renishaw InVia microRaman system. TGA was performed on a TG/DTA 320 (heating rate: 5 °C · min^{-1}). Nitrogen adsorption/desorption isotherms were measured at −196 °C by using a Micromeritics ASAP 2020 system. The samples were degassed at 150 °C overnight on a vacuum line.

Result and Discussions

As we show below, by changing the molecular weight of the block copolymer, we can control the pore sizes of the resulting crystalline TiO_2/carbon composites, denoted as CCM-TiO_2/carbon. Two different PI-*b*-PEO block copolymers were synthesized with standard anionic procedure. PI-*b*-PEO-1 with $\overline{M}_n = 27\,220$ g · mol^{-1}, 16.7 wt.-% PEO, and polydispersity index 1.02 and PI-*b*-PEO-2 with $\overline{M}_n = 15\,640$ g · mol^{-1}, 13.9 wt.-% PEO, and polydispersity index 1.03. PI-*b*-PEO-1 and PI-*b*-PEO-2 were subsequently used for the synthesis of composites CCM-TiO_2/carbon-1 and CCM-TiO_2/carbon-2, respectively, in a "one-pot" procedure as described in the Experimental Part.

During heat-treatment of as-made materials at 700 °C under nitrogen or argon atmosphere, most of the di-block copolymer is burned off, and amorphous TiO_2 and carbon precursors are converted to crystalline TiO_2 and conducting carbon, respectively, see Figure 1. Some of the polyisoprene of the di-block copolymer is also converted to conductive carbon.[14] SEM images of CCM-TiO_2/carbon-1 (Figure 2a) shows uniformly sized ≈20 nm sized open and accessible pores and the structure is short-range ordered reminiscent of wormhole-like structured mesoporous silica HMS.[15] TEM images of as-made material of CCM-TiO_2/carbon-1 corroborate the SEM results and already show the wormhole-like microphase separated structure which is preserved upon heating (see Figure 1S in Supporting

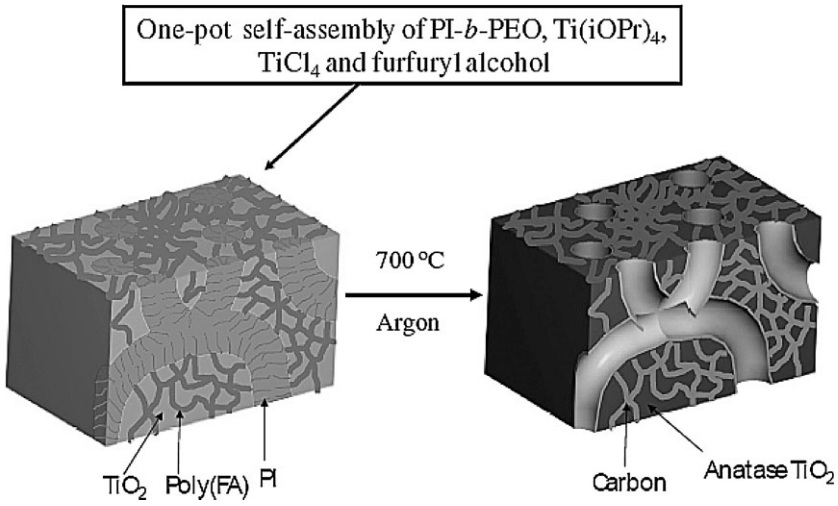

Figure 1. Schematic representation of "one-pot" synthesis of mesoporous crystalline TiO_2/carbon composites with large and uniform pores via carbonization of mesostructured PI-*b*-PEO/amorphous TiO_2/poly(furfuryl alcohol). The hexagonal arrangement of domains only serves for illustration purposes, see text.

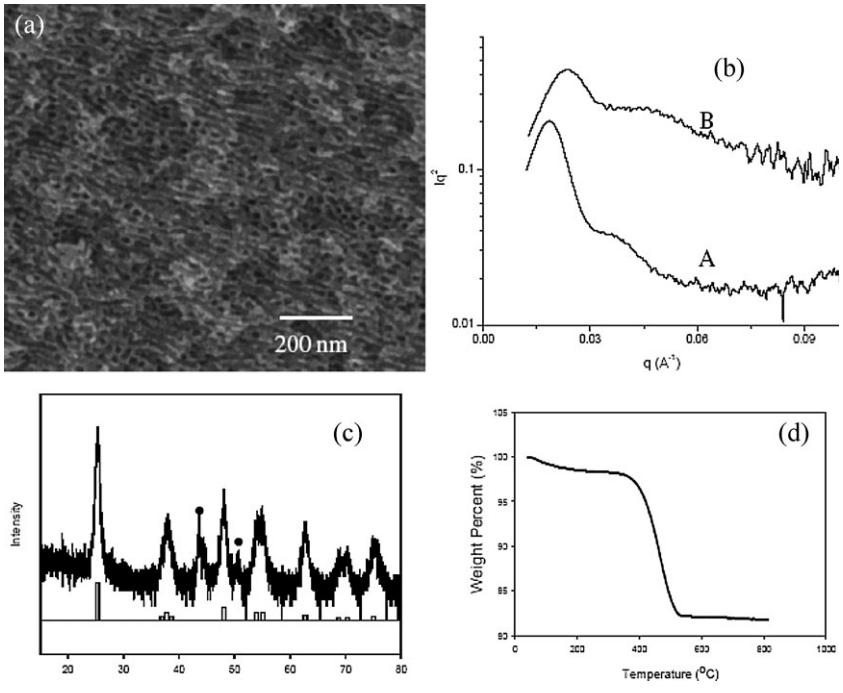

Figure 2. (a) SEM image of CCM-TiO_2/carbon-1; (b) SAXS traces of as-made composite (A) and CCM-TiO_2/carbon-1 (B); (c) powder XRD pattern of CCM-TiO_2/carbon-1. Bar markers signify the expected peaks for anatase TiO_2 structure (PDF 21-1276). Solid spheres indicate the peaks for aluminum substrate; (d) TGA data of CCM-TiO_2/carbon-1.

Information). Result of the SAXS characterization of the as-made and heat-treated materials is depicted in Figure 2b. For the as-made material, a first order peak is observed centered around values for the scattering wave vector, q, corresponding to a $d_{spacing}$ of 33.8 nm. The corresponding higher order peak is broad and unstructured which is typical for wormhole-like or short-range ordered hexagonal structures.[15] The wormhole-like structure is considered to be three-dimensionally interconnected, which is favorable for the diffusion of molecules inside the pores. After heat-treatment at 700 °C (see trace B in Figure 2b), the $d_{spacing}$ derived from the first order peak shifted to 26.6 nm, and the second order peak is preserved. The peak shift is the result of shrinkage of the structure during conversion of the carbon precursors to carbon and amorphous TiO_2 to crystalline anatase TiO_2. The formation of a crystalline oxide is evident from XRD analysis of the resulting materials (Figure 2c). Comparing peak positions with crystallographic databases identifies the material as the anatase phase of TiO_2 (PDF 21-1276). The average crystallite size as calculated from the Debye–Scherer equation is 7.8 nm.[16] Thermogravimetric analysis (TGA) of the heat-treated material run in air shows a 16% weight loss that occurs around 500 °C which is assigned to the oxidation of carbon in the pore walls, see Figure 2d. Raman spectra of the same material reveal the carbonaceous nature of CCM-TiO_2/carbon-1 with characteristic D-band (≈1 350 cm^{-1}) and G-band (≈1 600 cm^{-1}) (Figure 3). The intensity of D-band and G-band was much increased by increasing heat-treatment temperature from 450 to 700 °C, meaning that degree of graphitization was improved by heat-treatment at high temperature.

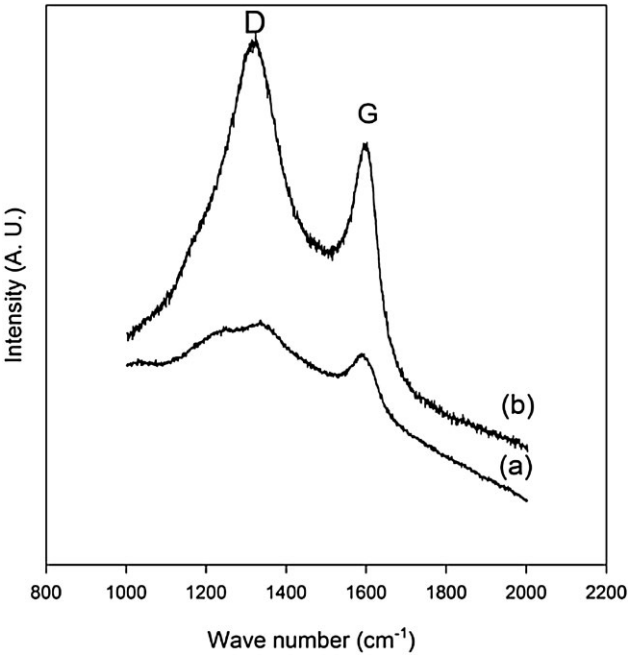

Figure 3. (a) Raman spectra of CCM-TiO_2/carbon-1 material heat-treated at 450 °C under N_2 (b) and CCM-TiO_2/carbon-1 heat-treated at 700 °C under air.

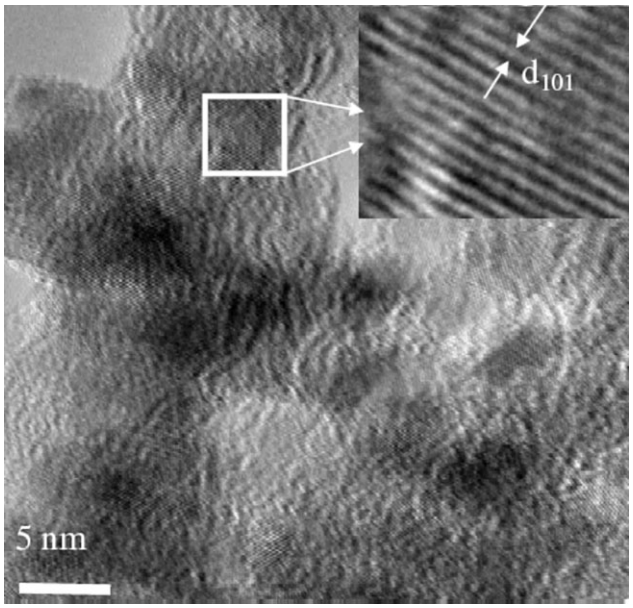

Figure 4. High-resolution TEM (HRTEM) image of CCM-TiO_2/carbon-1; inset: image showing d_{101} spacing of the anatase structure.

High-resolution TEM (HRTEM) of CCM-TiO_2/carbon-1 reveals that the walls are composed of small TiO_2 nanocrystals (Figure 4). The carbon might be present between TiO_2 crystals. For individual nanocrystals, a d_{101} spacing characterisitic for the anatase phase structure was clearly observed (Figure 4, inset).

To check whether the pores are open and accessible, nitrogen adsorption–desorption isotherms were measured on a Micromeritics ASAP 2020 at 77 K. In Figure 5,

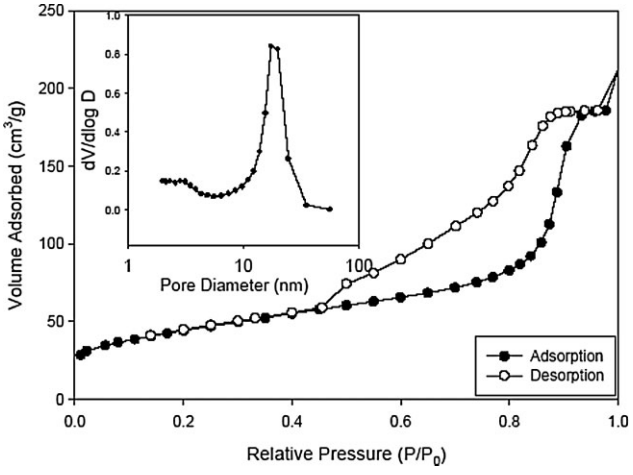

Figure 5. Nitrogen adsorption–desorption isotherms of CCM-TiO_2/carbon-1 with inset showing corresponding pore size distributions of CCM-TiO_2/carbon-1.

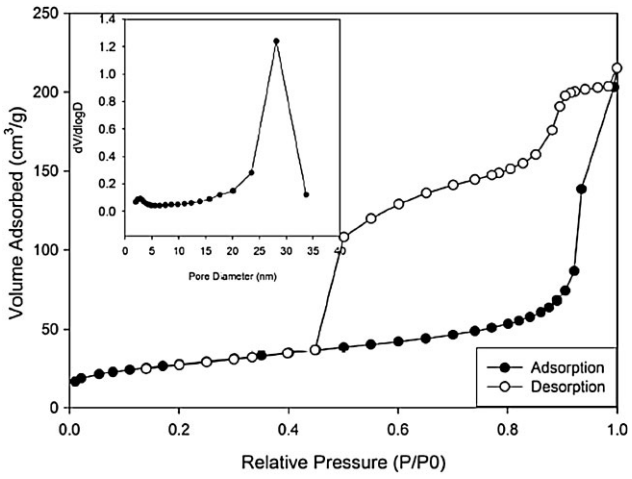

Figure 6. Nitrogen adsorption-desorption isotherms of CCM-TiO_2/carbon-1 material heat-treated at 450 °C under N_2, with inset showing corresponding pore size distributions. BET surface area and BJH pore size are 99 $m^2 \cdot g^{-1}$ and 28.1 nm, respectively.

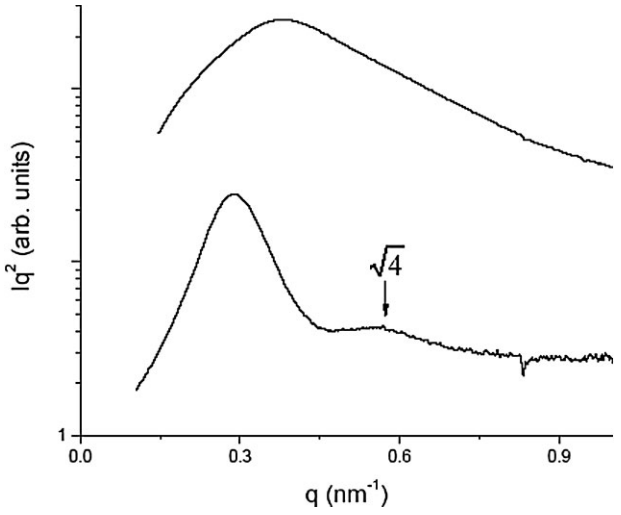

Figure 7. SAXS traces of as-made composite (a) and CCM-TiO_2/carbon-2 (b).

CCM-TiO_2/carbon-1 shows a nitrogen sorption isotherm of type IV according to the BDDT classification, with a specific surface area 154 $m^2 \cdot g^{-1}$ and a pore volume 0.3 $cm^3 \cdot g^{-1}$. Pore size calculations based on the BJH method reveal a pore diameter of 17.4 nm.[17] Such large pores are extremely important to provide access for large molecules during electrochemical processes. Using the four-point probe method, electrical conductivity of CCM-TiO_2/carbon-1 was measured under a pressure of 6.9 MPa (1 000 psi). As-made CCM-TiO_2/carbon-1 heat-treated at 450 °C under N_2 (Figure 6) lead to a conductivity value of 8.7×10^{-7} $S \cdot cm^{-1}$. This low conductivity is consistent with very weak carbon peaks in Raman scattering of this sample (Figure 3). In contrast, CCM-TiO_2/carbon-1 heat-treated at 700 °C under N_2 showed a conductivity of 9.4×10^{-3} $S \cdot cm^{-1}$. This considerably higher value is consistent with relatively well-developed G and D bands in Raman scattering spectra compared to those of the sample heat-treated at 450 °C. The conductivity value of CCM-TiO_2/carbon-1 is comparable to that of ordered mesoporous carbon materials derived from ordered mesoporous silica templates.[18] Furthermore, such high conductivities exclude the possibility that the carbon material is macro-phase separated and suggest that the conducting carbon is homogeneously mixed with TiO_2 nanocrystals in the mesostructured walls. Considering the density of anatase TiO_2 and carbon (density of anatase = 3.88 $cm^3 \cdot g^{-1}$, density of graphite = 2.27 $cm^3 \cdot g^{-1}$) and weight percentage of each material, the volume percentage of carbon should be at least 27%.[19]

By using block copolymer PI-*b*-PEO-2 with smaller molecular weight, a mesoporous TiO_2/carbon material with smaller pore size (denoted as CCM-TiO_2/carbon-2) was synthesized, demonstrating tunability of the pore size of the present mesoporous crystalline TiO_2/carbon composites. The SAXS results of the as-made and heat-treated materials (Figure 7) is again suggestive of a wormhole-like structure. For the as-made composite, a first order peak is observed centered around values for the scattering wave vector, q, corresponding a $d_{spacing}$ of 21.8 nm. The higher order peak is broad and unstructured which is typical for wormhole-like or short-range ordered hexagonal structures. After heat-treatment at 700 °C, a $d_{spacing}$ of the first peak was shifted to 17 nm, which is derived from shrinkage of structure during conversion of carbon precursor to carbon and amorphous TiO_2 to crystalline TiO_2.

From nitrogen adsorption–desorption isotherms (Figure 8a), the pore size and surface area are 8.2 nm and 144 $m^2 \cdot g^{-1}$, respectively. From powder XRD pattern (Figure 8b), the walls are also composed of crystalline anatase structure. Carbon content of this composite was 16 wt.-% as estimated from TGA under air.

Figure 9a shows the anodic performance of a composite electrode made from CCM-TiO_2/carbon-1. In order to examine the effect of carbon wiring, electrode from a pure mesoporous TiO_2 sample, referred to as CCM-TiO_2 (for detailed synthetic procedure and characterization, see the Experimental Part and Supporting Information)[14] was compared to CCM-TiO_2/carbon-1 composite electrode made without the carbon additive. In a typical electrode, carbon additive is included to enhance electrode conductivity. However, it is known that mixing large-sized conducting agents with porous materials is difficult due to a possible collapse of porous structure by conventional mixing techniques as well as inhomogeneous mixing, especially for large-scale production.[20] Note that both of the above electrodes were made without the carbon additive (Super P).

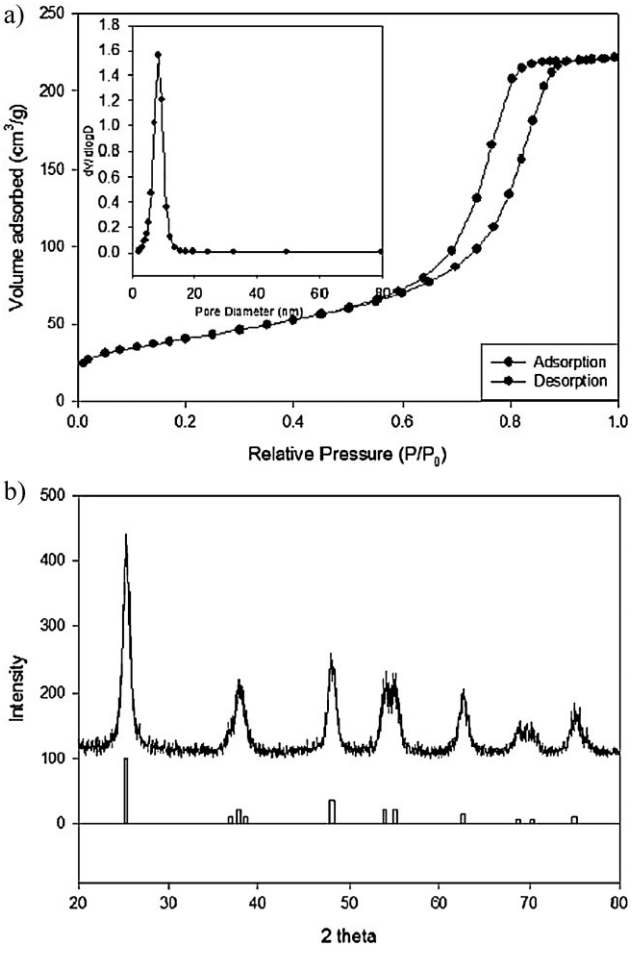

Figure 8. (a) Nitrogen adsorption–desorption isotherms of CCM-TiO_2/carbon-2, with inset showing corresponding pore size distributions. (b) Powder XRD pattern of CCM-TiO_2/carbon-2. Bar markers signify the peaks for anatase TiO_2 structure (PDF 21-1276).

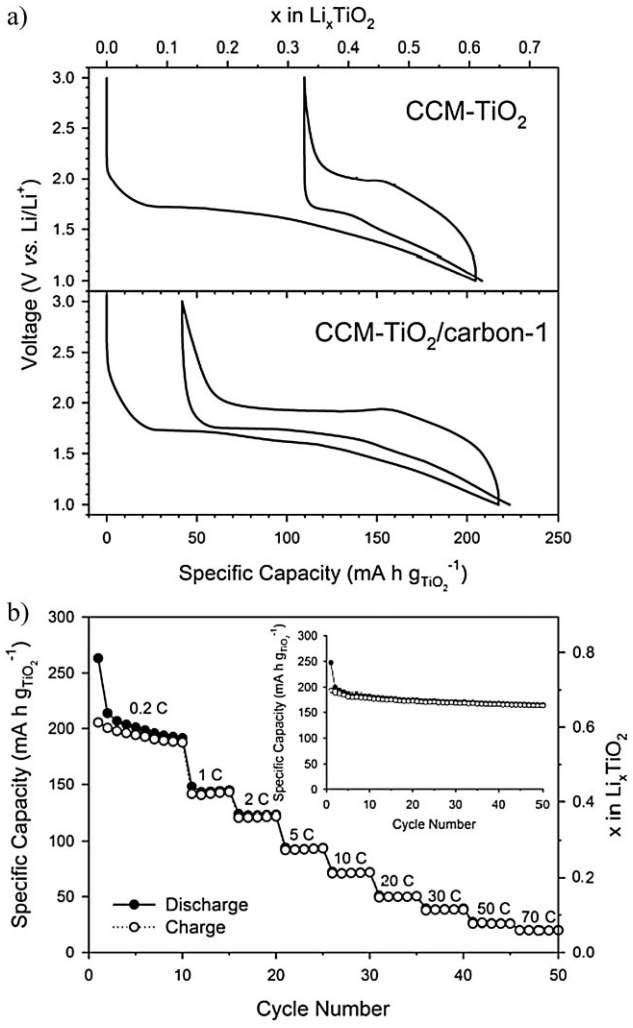

Figure 9. (a) Galvanostatic discharge–charge curves of CCM-TiO_2/carbon-1 and pure mesoporous TiO_2 electrodes cycled at a specific current of 0.2 C in the range of 1.0–3.0 V (vs. Li/Li^+); (b) Rate performance for CCM-TiO_2/carbon-1 electrode cycled at different rates. Cycle performance of CCM-TiO_2/carbon-1 electrode at 0.2 C is provided in the inset.

Electrodes were cycled with a specific current of 0.2 C in the range of 1.0–3.0 V (vs. Li/Li^+).

While the insertion capacity shows a similar value for the two samples (0.65 Li/Ti for CCM-TiO_2/carbon-1 and 0.60 Li/Ti for CCM-TiO_2), the desertion capacity of CCM-TiO_2 amounts to only 55% of that for CCM-TiO_2/carbon-1 (0.55 Li/Ti for CCM-TiO_2/carbon-1 and 0.30 Li/Ti for CCM-TiO_2). Anatase TiO_2 is known to react with Li transforming into lithium titanate, $Li_{0.5}TiO_2$, by a two-phase reaction [tetragonal (space group $I4_1/amd$) to orthorhombic (space group *Imma*) transition], wherein a decrease of the unit cell along the *c* axis and an increase of the *b* axis occurs with an overall 4% volume expansion.[21] The poorer desertion capacity of CCM-TiO_2 electrode, wherein there is no carbon component to fill the void spaces between TiO_2 particles, may be ascribed to a loss of electronic contact between TiO_2 particles, which is induced by such a volume change. The higher desertion capacity of CCM-TiO_2/carbon-1 electrode is then attributed to the presence of carbon component that plays as a conductive wire in TiO_2 frameworks. An evidencing feature for this assumption is the superior electronic conductivity of CCM-TiO_2/carbon-1 (9.4×10^{-3} $S \cdot cm^{-1}$) to that of CCM-TiO_2 (8.7×10^{-7} $S \cdot cm^{-1}$).

Figure 9b presents the cycle and rate performance of CCM-TiO_2/carbon-1 electrode. For providing sufficient conductive networks between particles and thereby achieving the best performance, the conducting aid (Super P, 12 wt.-%) was loaded in the composite electrodes. As shown in the inset, CCM-TiO_2/carbon-1 electrode exhibits a stable cycle performance. This could be due to the nano-size effect of grains, which allows a better accommodation of volume change upon insertion–desertion processes[21e] as well as stable electronic conduction paths through carbon wiring of the TiO_2 framework. It is also noticeable that TiO_2

in this electrode exhibits a high capacity (0.75 Li/Ti for insertion and 0.60 Li/Ti for desertion). Wagemaker et al. reported that the particle size of anatase TiO_2 has a striking impact on the Li insertion behavior.[22] Many studies on nano-sized or mesoporous TiO_2 show larger capacity than 0.5 Li/Ti, which has been accepted as the maximum insertion value at room temperature.[20,23–26] The higher capacity observed in the present work would thus be explained by this nano-size effect. For a test of the rate performance, the electrode was first cycled at 0.2 C for 10 cycles, and the rate was increased in stages to 70 C. The specific charge capacity at 30 C is 38 $mA \cdot h$ (g of TiO_2)$^{-1}$, which amounts to 18% of the first charge capacity. This value is much higher than that of the pure mesoporous TiO_2 electrode reported in ref. [26]. There is no doubt that a short diffusion length in a mesoporous structure is necessary for achieving a high rate capability because of the low diffusion coefficient (2×10^{-15} $cm^2 \cdot s^{-1}$) in the solid phase.[21c] A better rate capability that is achieved by shortening the diffusion length in mesoporous structure can be confirmed from the data obtained even at low current (0.2 C). The non-porous TiO_2 (BET surface area $\approx 0.2\ m^2 \cdot g^{-1}$), wherein the mesopores are collapsed due to high heat-treatment temperature (700 °C), is lithiated only up to 0.15 Li/Ti, which is far smaller than that for the CCM-TiO_2/carbon-1 electrode (Figure S3 of the Supporting Information). The electronic conduction is also a crucial factor on rate capability because of the insulating character of TiO_2.[20] Along this line, the conductive wiring of carbon on TiO_2 framework is believed to play a favorable role to give an excellent rate capability in this material, which is in accordance with other reports on the high rate capability of mesoporous TiO_2 composites with carbon nano-tubes (CNT)[20] or RuO_2.[26] However, to make such composite materials,[20,26] expensive CNTs or toxic cadmium ions should be added during synthesis. Furthermore, the resulting pore sizes are not well-defined but rather broad, making it impossible to study pore-size-dependent electrochemical properties.

Conclusion

In conclusion, mesoporous and highly crystalline TiO_2 (anatase)/carbon composites with large (>5 nm) and uniform pores were synthesized using PI-*b*-PEO block copolymers as structure directing agents. Pore sizes could be tuned by utilizing block copolymers with different molecular weights. The resulting mesoporous TiO_2/carbon was successfully used as an anode material for Li ion batteries. Without addition of conducting aid (Super P), the electrode showed high capacity during the first insertion/desertion cycle due to carbon wiring inside the walls of mesoporous TiO_2/carbon. The electrode further showed stable cycle performance up to 50 cycles and the specific charge capacity at 30 C was 38 $mA \cdot h$ (g of TiO_2)$^{-1}$, which indicates CCM-TiO_2/carbon can be used as a material for high rate use. We expect the CCM-TiO_2/carbon could also be used as a support for fuel cell electrode to reduce the amount of the expensive platinum metals.[27] The advantage of the present "one-pot"-type synthesis approach over previous work lies in its simplicity in terms of the necessary steps as well as the tunability of the resulting compositional as well as structural parameters. The latter provides an advanced materials platform toward energy generation and storage application.

Acknowledgements: This work was supported by the *Energy Materials Center at Cornell (EMC^2)*, an *Energy Frontier Research Center* funded by the *U.S. Department of Energy, Office of Science, Office of Basic Energy Sciences* under Award Number DE-SC0001086, and the *National Science Foundation* (DMR-0605856). The work was further supported by the *Korea Research Foundation Grant* funded by the Korean Government (MOEHRD) (KRF-2005-214-D00298), and by *KOSEF* via Research Center for Energy Conversion and Storage.

Received: November 5, 2010; Published online: January 7, 2011; DOI: 10.1002/macp.201000687

Keywords: batteries; carbon; composites; electrodes; mesoporous materials; synthesis

[1] [1a] M. S. Whittingham, *Chem. Rev.* **2004**, *104*, 4271; [1b] G.-Y. Adachi, N. Imanaka, S. Tamura, *Chem. Rev.* **2002**, *102*, 2405.
[2] [2a] J. Xi, J. Wang, L. Yu, X. Qiu, L. Chen, *Chem. Commun.* **2007**, 1656; [2b] K.-W. Park, K.-S. Ahn, Y.-C. Nah, J.-H. Choi, Y.-E. Sung, *J. Phys. Chem. B* **2003**, *107*, 4352.
[3] [3a] I. A. Courtney, J. R. Dahn, *J. Electrochem. Soc.* **1997**, *144*, 2045; [3b] Y. Wang, K. Takahashi, K. H. Lee, G. Z. Cao, *Adv. Funct. Mater.* **2006**, *16*, 1133; [3c] S. J. Han, B. C. Jang, T. Kim, S. M. Oh, T. Hyeon, *Adv. Funct. Mater.* **2005**, *11*, 1845.
[4] [4a] Y. G. Guo, Y.-S. Hu, J. Maier, *Chem. Commun.* **2006**, 2783; [4b] Z. Zhang, Z. Gong, Y. ang, *J. Phys. Chem. B* **2004**, *108*, 17546.
[5] M. A. Reddy, M. S. Kishore, V. Pralong, V. Caignaert, U. V. Varadaraju, B. Raveau, *Electrochem. Commun.* **2006**, *8*, 1299.
[6] [6a] C. K. Chan, H. Peng, G. Liu, K. Mcilwrath, X. Feng, Z. Robert, A. Huggins, Cui. Yi, *Nat. Nanotechnol.* **2008**, *3*, 31; [6b] B. Gao, S. Sinha, L. Fleming, O. Zhou, *Adv. Mater.* **2001**, *13*, 816.
[7] [7a] J. Li, S. Tang, L. Lu, H. C. Zeng, *J. Am. Chem. Soc.* **2007**, *129*, 9401; [7b] I. Grigoriants, L. Somoinski, L. Hongliang, I. Ifagarga, D. Aurbach, A. Gedanken, *Chem. Commun.* **2005**, 921; [7c] S. Zhu, H. Zhou, M. Hibino, I. Honma, M. Ichihara, *Adv. Funct. Mater.* **2005**, *15*, 381; [7d] J. Fan, T. Wang, C. Yu, B. Tu, Z. Jiang, D. Zhao, *Adv. Mater.* **2004**, *16*, 1432.
[8] [8a] P. Yang, D. Zhao, D. I. Margolese, B. F. Chmelka, G. D. Stucky, *Nature* **1998**, *396*, 152; [8b] M. Zukalova, A. Zukal,

L. Kavan, M. K. Nazeeruddin, P. Liska, M. Gratzel, *Nano Lett.* **2005**, *5*, 1789.
[9] R. Liu, Y. Ren, Y. Shi, F. Zhang, L. Zhang, L.B. Tu, D. Zhao, *Chem. Mater.* **2007**, *20*, 1140.
[10] H. Tamai, M. Kouzu, M. Morita, H. Yasuda, *Electrochem. Solid-State Lett.* **2003**, *6*, A214.
[11] Y. Meng, G. Dong, F. Zhang, Y. Shi, H. Yang, Z. Li, C. Yu, B. Tu, D. Zhao, *Angew. Chem., Int. Ed.* **2005**, *44*, 7053.
[12] S. Acosta, R. Corriu, D. Leclercq, P. H. Mutin, A. Vioux, *J. Sol-Gel Sci. Technol.* **1994**, *2*, 25.
[13] [13a] M. Templin, A. Franck, A. Du Chesne, H. Leist, Y. Zhang, R. Ulrich, V. Schädler, U. Wiesner, *Science* **1997**, *278*, 1795; [13b] S. C. Warren, F. J. DiSalvo, U. Wiesner, *Nat. Mater.* **2007**, *6*, 156.
[14] J. Lee, M. C. Orilall, S. C. Warren, M. Kamperman, F. J. DiSalvo, U. Wiesner, *Nat. Mater.* **2008**, *7*, 222.
[15] [15a] P. T. Tanev, T. J. Pinnavaia, *Science* **1995**, *267*, 865; [15b] J. Lee, S. Yoon, S. M. Oh, C.-H. Shin, T. Hyeon, *Adv. Mater.* **2000**, *12*, 359.
[16] A. D. Krawitz, *Introduction to Diffraction in Materials Science and Engineering*, John Wiley & Sons, Inc, New York 2001, p. 168.
[17] J. H. de Boer, *The Structure and Properties of Porous Materials*, Butterworths, London 1958.
[18] C. H. Kim, D.-K. Lee, T. J. Pinnavaia, *Langmuir* **2004**, *20*, 5157.
[19] The actual density of carbon is lower than that of graphite because of the micropores in amorphous carbon and larger $d_{spacing}$.
[20] I. Moriguchi, R. Hidaka, H. Yamada, T. Kudo, H. Murakami, N. Nakashima, *Adv. Mater.* **2006**, *18*, 69.
[21] [21a] R. J. Cava, D. W. Murphy, S. Zahurak, A. Santoro, R. S. Roth, *J. Solid State Chem.* **1984**, *53*, 64; [21b] T. Ohzuku, T. Kodama, T. Hirai, *J. Power Sources* **1985**, *14*, 153; [21c] R. van de Krol, A. Goosens, J. Schoonman, *J. Phys. Chem. B* **1999**, *103*, 7151; [21d] M. Wagemaker, G. J. Kearley, A. A. van Well, H. Mutka, F. M. Mulder, *J. Am. Chem.* **2002**, *125*, 840; [21e] G. Sudant, E. Baudrin, D. Larcher, J.-M. Tarascon, *J. Mater. Chem.* **2005**, *15*, 1263.
[22] M. Wagemaker, W. J. H. Borghols, F. M. Mulder, *J. Am. Chem. Soc.* **2007**, *129*, 4323.
[23] L. Kavan, M. Kalbác, M. Zukalová, I. Exnar, V. Lorenzen, R. Nesper, M. Graetzel, *Chem. Mater.* **2004**, *16*, 477.
[24] X. Gao, H. Zhu, G. Pan, S. Ye, Y. Lan, F. Wu, D. Song, *J. Phys. Chem.* **2004**, *108*, 2868.
[25] Y. G. Guo, Y. S. Hu, J. Maier, *Chem. Commun.* **2006**, 2783.
[26] Y. G. Guo, Y. S. Hu, W. Sigle, J. Maier, *Adv. Mater.* **2007**, *19*, 2087.
[27] S. Shanmugam, A. Gedanken, *Small* **2007**, *3*, 1189.